Available online at www.eccomasproceedia.org
Eccomas Proceedia COMPDYN (2017) 3476-3490

ECCOMAS
Proceedia

COMPDYN 2017
6th ECCOMAS Thematic Conference on
Computational Methods in Structural Dynamics and Earthquake Engineering
M. Papadrakakis, M. Fragiadakis (eds.)
Rhodes Island, Greece, 15–17 June 2017

NONLINEAR FEA OF SOIL-STRUCTURE-INTERACTION EFFECTS ON RC SHEAR WALL STRUCTURES

Mohammad AlHamaydeh, Ph.D., P.E.[1], George Markou, Ph.D.[2], and Dina Saadi[1]

[1] American University of Sharjah
PO Box 26666, Sharjah, United Arab Emirates
e-mail: malhamaydeh@aus.edu, g00037041@aus.edu

[2] ALHOSN University
PO Box 38772, Abu Dhabi, United Arab Emirates
e-mail: g.markou@alhosnu.ae

Keywords: Nonlinear, FEA, Reinforced Concrete, Soil-Structure-Interaction.

Abstract. *Considering Soil-Structure-Interaction (SSI) in Finite Element Analysis (FEA) is accounted for through explicit representation of the soil domain allowing for departures from fixed base conditions and constraints. The performance evaluation of a six-story reinforced concrete (RC) shear wall with and without SSI is presented in this paper. The soil domain and Reinforced Concrete (RC) elements including walls, slabs, and foundations are modeled using 3D 8-noded hexahedral brick elements. Furthermore, longitudinal and transverse reinforcement are modeled as embedded rod elements while the cracking of concrete is modeled via the smeared crack approach. Nonlinear pseudo-static and cyclic pushover analyses are carried out on fixed and flexible base models. The soil in the flexible base model represents a site class E soil type according to ASCE7-10. A parametric study is performed on different pushover loading profiles prior to the comparison between fixed and flexible base systems. The performance evaluation of the two systems is done through direct comparison of pushover curves, displacement, strain locations and cracking patterns. Based on the numerical findings, the RC wall in the SSI model is found to exhibit higher lateral displacements yet lesser levels of strain concentrations for the any given horizontal deformation. Additionally, the superstructure toughness developed in the fixed base model is higher than the SSI model due to the vertical displacement of the soil medium. Finally, cracks in the slabs are found to be more prominent in the SSI model at the upper floors due to the accumulated lateral displacement of the wall and the overall more flexible behavior of the model. In conclusion, soil flexibility (SSI) is found to have a considerable effect on the overall structural system behavior.*

Peer-review under responsibility of the organizing committee of COMPDYN 2017.
doi: 10.7712/120117.5659.18218

1 INTRODUCTION

Considering soil flexibility during analysis for any structural system will result in different stress distributions and displacement profiles. Soil-Structure Interaction (SSI) evaluates the structural system response taking into account the soil as a support condition. Soil deformability often leads to releasing stresses in footings that will increase lateral displacements. The extent of soil deformability depends on many parameters, such as bearing capacity, shear wave velocity, cohesion, etc.

Two mechanisms have to be considered when studying the impact of SSI on the seismic response of structures, kinematic interaction and inertial interaction. Kinematic interaction is the mechanism that occurs due to difference in movement between the soil and foundation. Inertial interaction is the mechanism induced from the relative displacement between the soil and foundation due to the inertial forces. Inertial forces cause base shear and moments at the foundation level that could cause displacement to the soil [1].

The simulation of the soil medium by using Finite Element Analysis (FEA) is essential when considering the SSI phenomenon. To obtain accurate results, the soil element mesh size has to be optimized in order to obtain accurate results with reasonable computational demand. Similarly, the extent of the soil medium and its representative depth has to be wisely chosen if large models and excessive computational demands are to be avoided.

Tabatabaiefar et al. [2] used 2D Finite Element (FE) modeling in order to study the seismic behavior of a ten-story building with a moment-resisting frame considering SSI effects. Their SSI model included the discretization of the soil depth utilizing shell elements, while the building's frame was modeled through the use of beam-column linear elements. The used software was FLAC2D, which is a 2D FE software that can model the soil profile with different shear wave velocities representing soil classes such as Ce, De and Ee according to the Australian code. Likewise, a nonlinear elasto-plastic constitutive SSI model was investigated by Torabi and Rayhani [1] by using a 3D FE model. Different embedment depths and aspect ratios were considered when discretizing the soil domain so as to account for SSI. The 3D modeling of soil medium was done in Opensees with 8-noded brick elements with total depth of 30m. The superstructure was modeled as lumped mass SDOF beam-column element for simplicity and computational efficiency purposes.

A more recent work was presented by Markou and AlHamaydeh [3] and Makrou et al. [4], in the latter, the full-scale five-story RC building was modeled under pseudo-static push over loads. The soil domain, the raft slab and half of the ground floor of the structure were modeled through the use of the 8-noded solid elements, while the remaining part of the superstructure was modeled through the use of the beam-column finite element that incorporates the fiber approach and the natural mode method. This type of simulation is known as hybrid modeling (HYMOD) which allows for the decrease of the computational demand without losing the required numerical accuracy during the analysis.

Nonlinear FEA (NLFEA) is pivotal to earthquake engineering [5]–[18] and failure analysis [19], [20]. The available tools for the structural engineering community vary significantly in complexity and capability. Since high fidelity NLFEA is typically very demanding computationally, brilliant simplifications are always sought after. Some of the common and widely accepted methods are macromodel-based formulations which implement comprehensive elements capable of exhibiting nonlinear characteristics. Macromodel-based formulations either incorporate fiber models to calculate member properties, they are based on mechanics of typical structural members. Common nonlinearities that are accommodated by such techniques are:

linear or uniform flexibility, as well as concentrated or distributed plasticity with yield penetration, etc. Many existing analysis platforms employ such modeling capabilities. e.g. IDARC-2D [21], [22], OpenSees [23]–[25], ZeusNL [26] and SeismoStruct [27].

2 PROBLEM DESCRIPTION

2.1 Structure properties

This paper will focus on examining the lateral response of a six-story RC shear wall including the associated tributary areas of the slabs, and considering SSI effects. Two FE models are investigated herein, a fixed base model and a flexible base model. Figure 1 shows the fixed base model. The FE model includes a shallow foundation, the shear wall, six slabs and a soil medium (for the case of the flexible base model; see Figure 2). Furthermore, the wall and slab reinforcement are discretized and modeled as shown in Figure 1b. The considered RC wall was designed and detailed as ordinary RC wall in accordance to the ASCE7-10 standard [28]. The design and detailing of the RC wall was adopted from a previously conducted investigation [12]. The RC wall is 2.5 m long in-plan and 24 m in height (six floors at 4 m). Table 1 summarizes the remaining design specifics. The considered building, from which the representative RC shear wall is used herein, was designed to sustain a superimposed dead load of 3.6 kPa (75psf), live load of 2.4 kPa (50psf), and partition wall load of 0.72 kPa (15psf). The FE modeling and analysis are carried out using the ReConAn FEA solver [29].

Table 1- Design details for the RC shear wall

Element/Floors	Compressive Strength (MPa)	In-Plan Length x Thickness (mm)	Vertical (Flexural) Reinforcement	Horizontal (Shear) Reinforcement
Walls/4-6	38	2500x200	T12@450mm	T12@450mm
Walls/1-3	38	2500x250	T25@200mm	T16@300mm
Slabs/1-6	28	200	T16@150mm top and bottom	

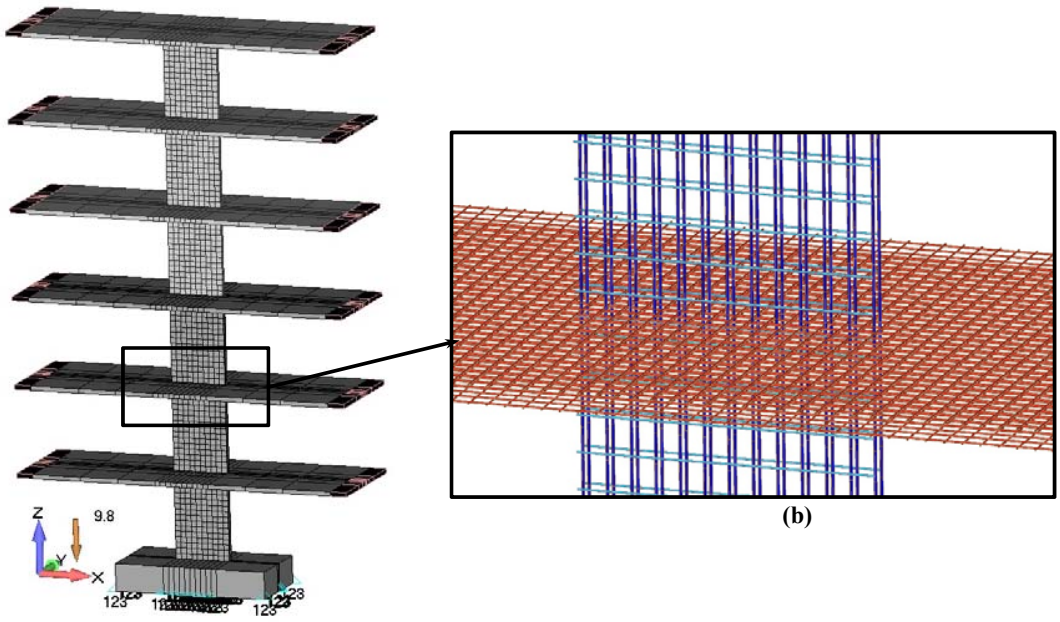

Figure 1- Finite Element Mesh of the fixed base model (a) Concrete hexahedral elements, (b) Embedded rebar elements

2.2 Soil properties

The soil extent is taken as two times the foundation in-plan dimensions in the lateral and longitudinal directions as recommended in the literature [30]. The foundation footprint is 3.5 m by 7 m, and 1.25 m deep. Based on the adopted soil domain dimensions, the model included a total soil depth equal to 10 m. Figure 2 illustrates the discretization of the soil medium created in order to account for the SSI effects in the flexible base model. The top of foundation is matching the top of soil and does not assume any above-foundation soil, a simplified conservative modeling approach.

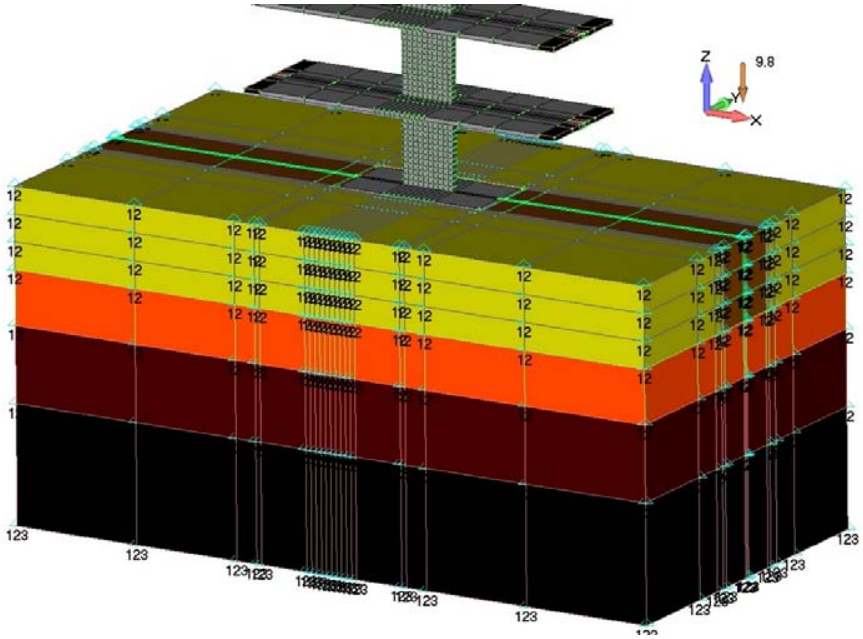

Figure 2- Finite element mesh of the flexible base model

In regards to the soil parameters, Table 20.3-1 of ASCE7-10 [28] was used where the soil characteristics (shear wave velocity and standard penetration resistance) of site class E were adopted. Using basic soil parameters, the bearing capacity and modulus of elasticity of the soil are calculated using equations 1 through 4 [31] (see Table 2).

$$G = {v_s}^2 \times \rho \quad (1)$$

$$E = 2(1+\mu)G \quad (2)$$

$$\emptyset\,(\text{deg}) = 27.1 + 0.3\text{N}_{60} - 0.00054\,(\text{N}_{60})^2 \quad (3)$$

$$q_u = q \times N_q + 0.5 \times \gamma \times B \times N_\gamma \quad (4)$$

G	Shear modulus	$\emptyset$	Soil internal friction angle	γ	Soil unit weight
E	Modulus of elasticity	N_{60}	Standard penetration resistance	B	Footing width
v_s	Shear wave velocity	N_q /N_γ	Terzaghi's bearing capacity factors	q_u	Soil bearing capacity
ρ	Soil density	q	Soil pressure underneath footing	μ	Poisson's ratio

Table 2- Soil parameters for site class E

Soil Parameter	G	E	$\emptyset$	q_u
Value	25.3 MPa	65.7 MPa	28.9°	0.964 MPa

3 VALIDATION MODEL

The validation process was performed through numerical calibration of the FEA model against published experimental results. The SSI problem that was adopted in this investigation was adopted from Lin et al. [32], where the effects of biogrouting on concrete piles embedded in sandy soils was investigated. In one experiment, a 76 mm-diameter concrete pile was embedded in sandy soil medium extending 1.1m by 1.1 m and 1.55 m deep. The pile was pushed down along the gravity direction until failure. The soil had sensors in different locations to capture stresses and displacements. The vertical load versus the vertical displacement plot for a non-treated pile was compared with the curve obtained from the simulation model developed in this presented research. Figure 3a shows the FE model of the concrete pile embedded in soil, while Figure 3b illustrates the displacement of the concrete pile inside the soil medium. The soil elements that were connected to the pile were modeled assuming a low compressive strength and modulus of elasticity in an attempt to capture the shear stresses that are transferred from the pile to the sand domain through friction.

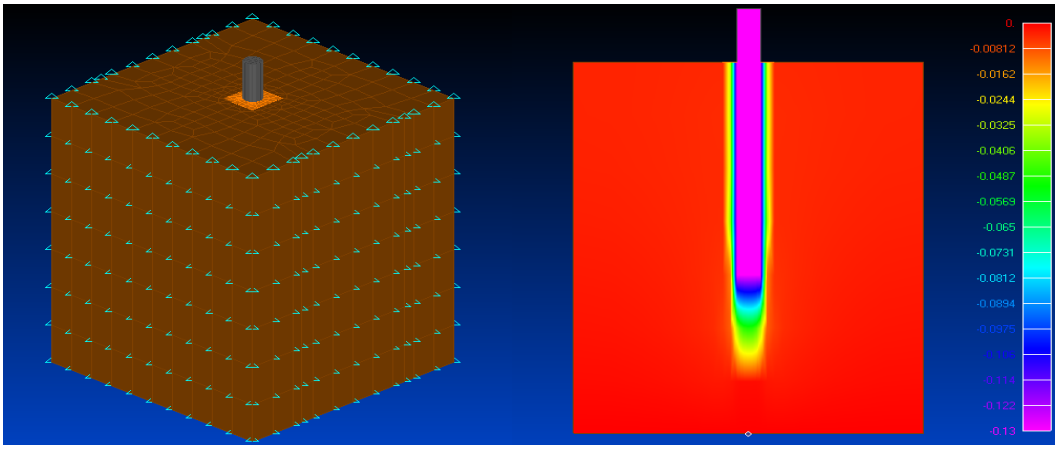

(a) **(b)**

Figure 3- Concrete pile embedded in sand domain (a) 3D mesh of pile and soil medium, (b) displacement contour just prior to failure

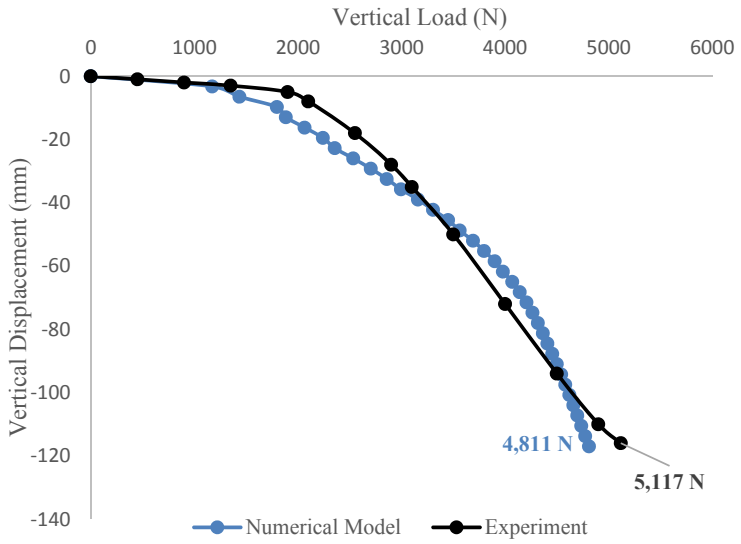

Figure 4- Comparison between the numerical and experimental for vertical load vs pile displacement

The comparison between the experimental and numerical results is shown in Figure 4. From the comparison is clearly observed that the numerical model captures the essence experimentally reported mechanical behavior.

4 NONLINEAR FEA

4.1 Modeling assumptions

In order to account for the continuity of slabs and avoid cantilever-type deformations, the tributary area associated with the wall is modeled with roller restraints around the edges. Figure 5 shows the restraints assigned to the slabs where the same boundary conditions were applied at all floors. Given that the horizontally applied displacements and forces during the analyses, were along the x-axis of the model, the z- and y-axis Degrees Of Freedom (DOFs) were fixed along the edges of the short span of the slabs (parallel to the y-axis), while the edges found on the long span of the slabs were restrained in the y-axis in order to avoid any out of plane deformations.

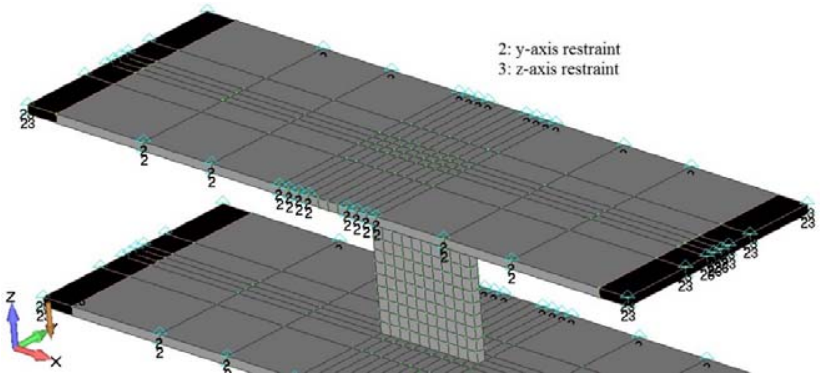

Figure 5- Slab boundary conditions

4.2 Loading protocol

The modeled structure was loaded with lateral displacements along the x-axis (displacement-control) and the members' own weights were accounted for by the software automatically. Superimposed gravity loads (dead and live) were applied as distributed loads on the slabs. Displacement-controlled pushover analysis was performed so as to evaluate the overall system's seismic response (Soil-Foundation-Wall). Since the seismic loads originate at the slab center of mass and then are transmitted to the lateral forces-resisting system (wall), the imposed displacements were assigned at the floor levels. The relative magnitudes of the assigned displacements were kept constant and proportional to floor elevations, so as to simulate the induced inertial forces during seismic events [33]. In this presented research work the building is pushed laterally for a maximum roof displacement of 2.5% of its total height (600 mm). Since the distribution of the prescribed seismic loads/displacements greatly influences the capacity estimates for the structure at question, a parametric study was performed. It is generally recommended to consider at least two different profiles [33]. Therefore, four different displacement profiles were considered in an effort to shed light on any design weaknesses that static analyses are incapable of detecting. Equation 5 describes the displacement applied at each floor for all considered profiles, where ($\boldsymbol{x}$) is the floor elevation from ground level, ($\boldsymbol{L}$) is the total building height and ($\boldsymbol{k}$) is the profile power factor ranging from 1 to 2. Specifically, the four profiles had the following power factors: 1 (linear first fundamental vibrational mode), 1.2 (profile used for the

original design), 1.5 and 2 (typical cases to be considered representing higher mode effects to different extents). This sensitivity analysis exercise was performed on the fixed-base model only for brevity.

$$Floor\ Displacement = (\frac{x}{L})^k \tag{5}$$

The pushover curves were compared as shown in Figure 6. For k = 1 and 2, the profiles were deemed not very suitable, as the former uncooperatively exaggerates the capacity while the latter unrealistically underestimates the capacity since it is associated with extreme higher-modes-dominated behavior. For k = 1.2 and 1.5, they are deemed appropriate seismic capacities for the structural system. The k value of 1.2 is chosen as it is consistent with the design stage profile for the original building [12].

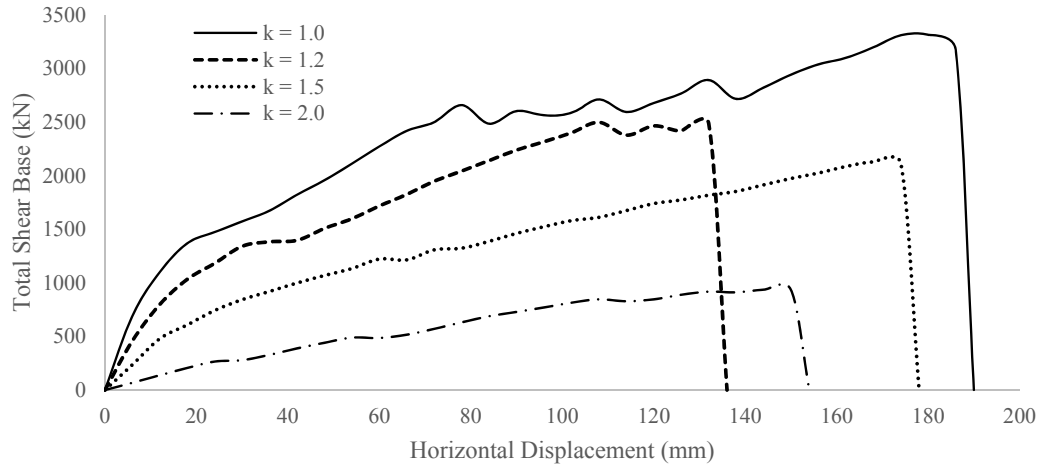

Figure 6 - Pushover curves for different displacement profiles

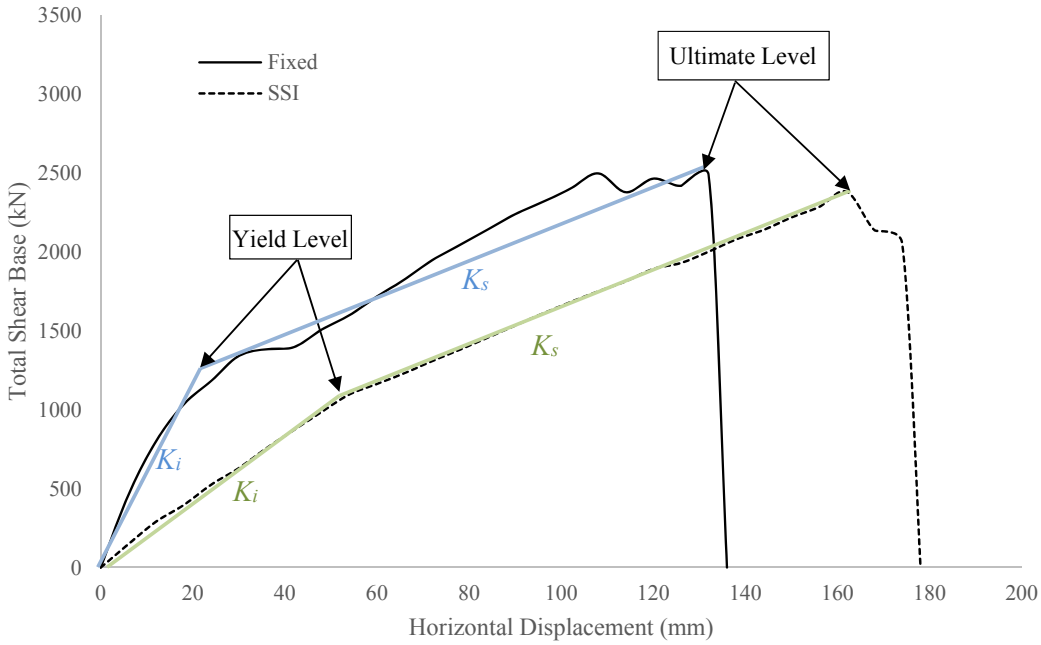

Figure 7 – Base shear vs horizontal displacement curves for the fixed base and SSI models

The following comparisons between the fixed base and flexible base models including displacements, strains and cracking patterns, are based on the k = 1.2 displacement profile. Figure 7 demonstrates the pushover curves of two models as they were subjected to the same displacement-controlled pseudostatic protocol.

5 DISCUSSION OF RESULTS

5.1 Pseudostatic Pushover Loading

5.1.1. Force-Deflection Response

Changing the fixed boundary conditions applied at the foundation level with hexahedral finite elements (soil base) allows the isolated footing to compress the soil resulting in a more flexible structural response. Consequently, rotation is allowed at the base which leads to increased lateral displacements (corresponding to some internal stresses relieves) in the superstructure. In this article, the pushover analysis was performed using displacement-controlled approach where the building was pushed laterally to 2.5% of the total height, which is 0.025 x 24m = 0.6m. The imposed displacement was applied through the use of 100 displacement increments and an energy-based convergence criterion tolerance equal to 10^{-5}. Referring to the pushover curves in Figure 7, the fixed base model demonstrates higher resistance for any specific imposed displacement value. Key response parameters, such as the initial stiffness ($\boldsymbol{K_i}$) and secondary stiffness ($\boldsymbol{K_s}$) for the fixed base and SSI models are evaluated and listed in Table 3.

$$K_i = \frac{Fy}{\Delta y} \tag{6}$$

$$K_s = \frac{Fu - Fy}{\Delta u - \Delta y} \tag{7}$$

Where Fy is the yield force, Fu is the ultimate force, Δy and Δu are the yield and ultimate displacements, respectively.

Generally, the SSI model exhibits more flexible behavior in comparison to the fixed base model (higher displacements corresponding to lower forces). For example, the yield displacement is 225% higher for the SSI model, and the initial stiffness is 41% lesser, compared to their fixed base counterparts. Since lesser stress and strain demands are typically undergone in the SSI model, the yield force is also lesser, but the secondary stiffness is higher. This is indicative of lesser superstructure inelastic demands exhibited through higher post-yielding stiffness. Moreover, the superstructure toughness is reduced by 16%.

Table 3- Key response parameters from Figure 7

Parameter	SSI Model	Fixed Base (FB) Model	SSI/FB
Fy	1,098 kN	1,183 kN	0.93
Δy	0.054m	0.024m	2.25
K_i	20,333 kN/m	49,292 kN/m	0.41
Fu	2,382 kN	2,488 kN	0.96
Δu	0.162m	0.132m	1.23
K_s	11,889 kN/m	12,083 kN/m	0.98
K_s / K_i	0.585	0.245	2.39
Toughness	235 kJ	249 kJ	0.94

Figure 8 shows the numerically predicted deformed shapes for the two models at the ultimate loading conditions. As it can be seen the fixed base model failed at a total horizontal displacement of 136 mm, where the corresponding displacement for the case of the SSI model was 169 mm (24.3% larger displacement prior to failure).

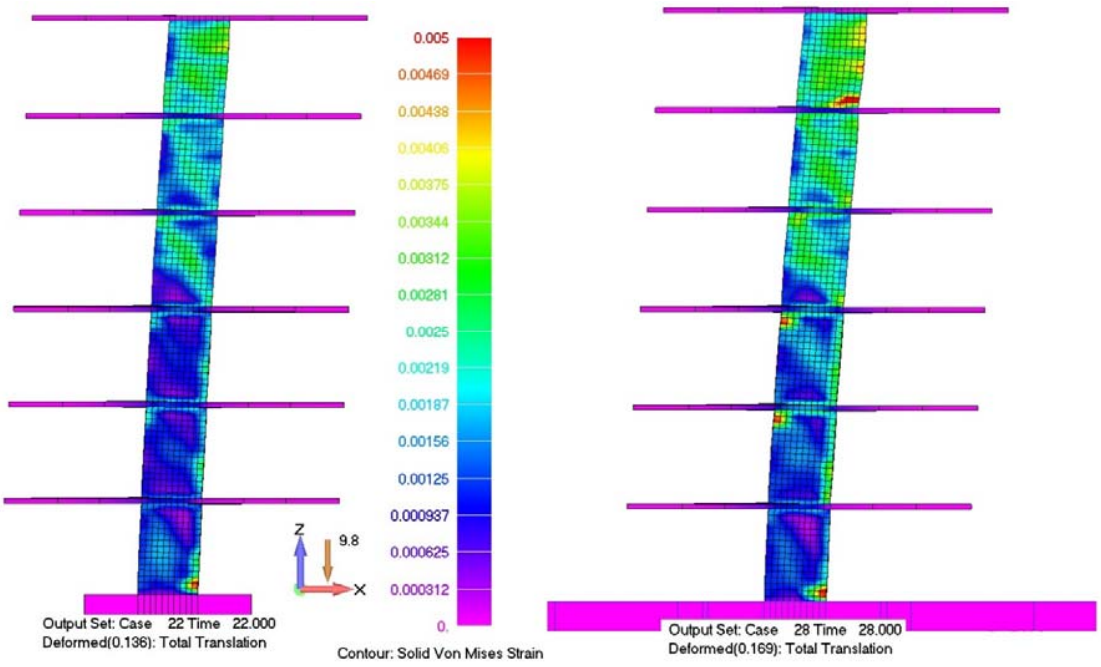

(a) **(b)**

Figure 8 – Von Mises strain contours on deformed shape prior to failure of the (a) SSI model (b) fixed base model.

5.1.2. Strain levels

Based on the numerical findings, the strain concentrations in the RC wall of the fixed model were found to be higher in the fixed base model due to their high stiffness. This is expected given the boundary conditions that were applied at the foundation level which does not allow for any rotation. Figure 8 illustrates the differences in strain levels prior to failure for the two models. As it can be seen, for the case of the SSI model the lower floors exhibited lower strain concentrations in comparison to the fixed model at the stage of the maximum horizontal displacement. This is attributed to the ability of the SSI model to allow the isolated footing to develop rotations (Figure 8b). The strains shown in indicate the high demands from the pushover analysis, as strain values above 0.003 indicates that the concrete sections are tension-controlled and exhibiting significant yielding according to ACI318-11, Chapter 9 [34].

Moreover, the numerical investigation showed that the fixed base model exhibited a cracking pattern that is dominated by horizontal and diagonal cracks at the bottom region of the RC wall due to the full rotational restraint of the base. At the point where the maximum horizontal displacement was applied, the isolated footing developed tensile cracks as well. The full restraint of the foundation creates high moments that cause cracking of concrete due to tensile stress concentrations. Whereas in the SSI model, the crack development in the slabs was found to be higher. This finding could be attributed to the increased lateral wall displacements as a direct result of the rotational flexibility of its base. i.e. the additional sway of the wall adds more bending demands on the slabs given the relative rigidly of the wall.

5.2 Cyclic Loading

5.2.1. Force-Deflection Response

Cyclic displacement-controlled analysis was performed to further investigate the overall effect of the SSI phenomenon in terms of the overall structural behavior of the considered system. The lateral displacement protocol that was imposed on the structure pictorially illustrated in Figure 9. The resulting hysteretic loops obtained from the analysis can be seen in Figure 10. It is observed that the force-deformation curves in Figure 10 indicate a somewhat similar seismic response to that presented in Figure 7. The deterioration in the structural response after the first two cycles, can be easily noticed. The cyclic structural toughness (area enclosed in hysteresis loops) the fixed base and SSI models were found to be 677.45 kJ and 643.27 kJ, respectively. The 5% reduction in the cyclic structural toughness is evidently a direct consequence of the increased flexibility of the SSI model.

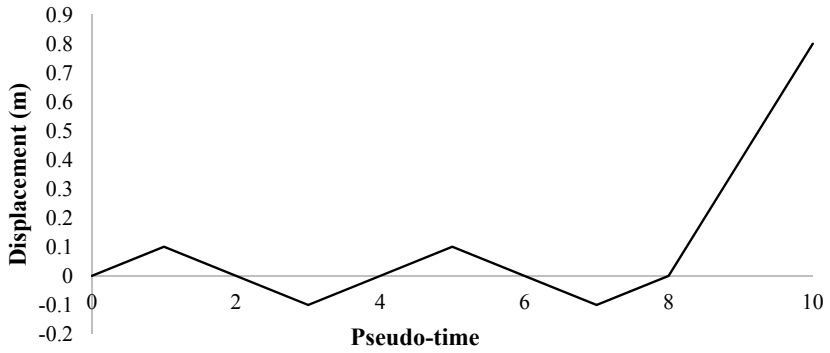

Figure 9- Cyclic lateral displacement protocol

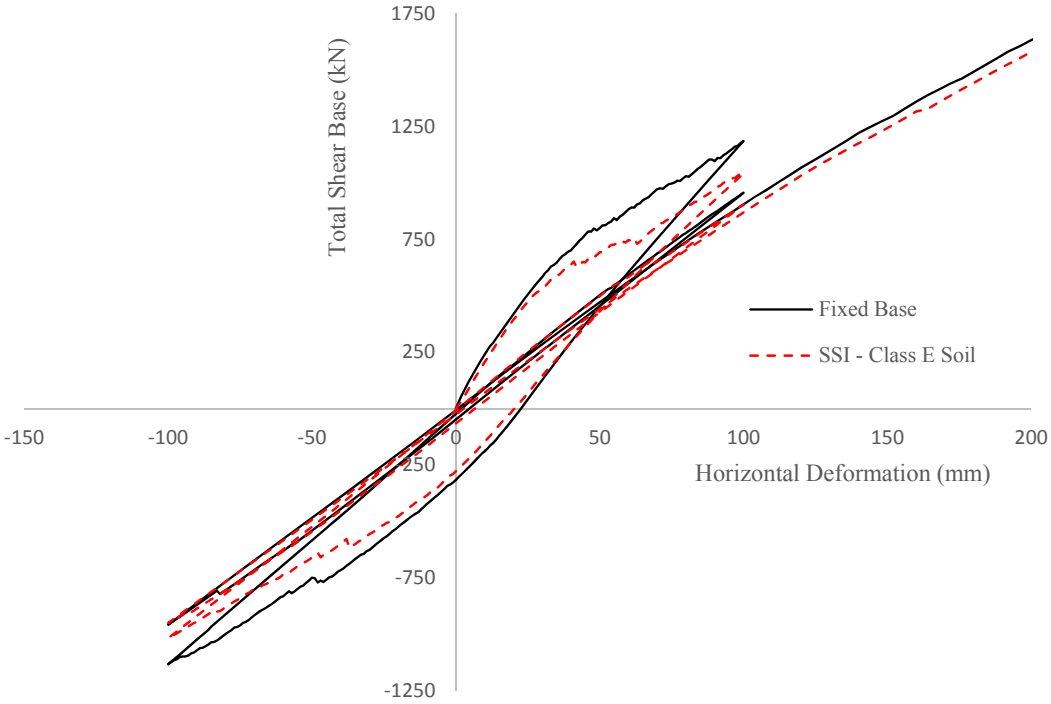

Figure 9- Hysteresis curve for fixed base and flexible base models

Figures 11 illustrate the Von Mises strain levels for the cyclic analysis of flexible base model at a roof displacement of 0.2m. The cyclic analysis material models that were used to perform this numerical investigation were based on the work presented by Mourlas et al. [35].

5.2.1. Soil Stress-Strain Response

The soil's contribution to the overall structural behavior was evident for the analyses performed with the SSI model. Stress concentrations at various locations were captured throughout the cyclic analysis. As it can be seen in Figures 12 and 13, the von Mises stresses that were developed under the foundation were not larger than 200 kPa, which indicates that the soil domain behaved in a linear manner throughout the analysis. In addition to that, it is easy to observe that the stress contours in the soil medium are controlled by the deformation state of the shear wall structure and its foundation.

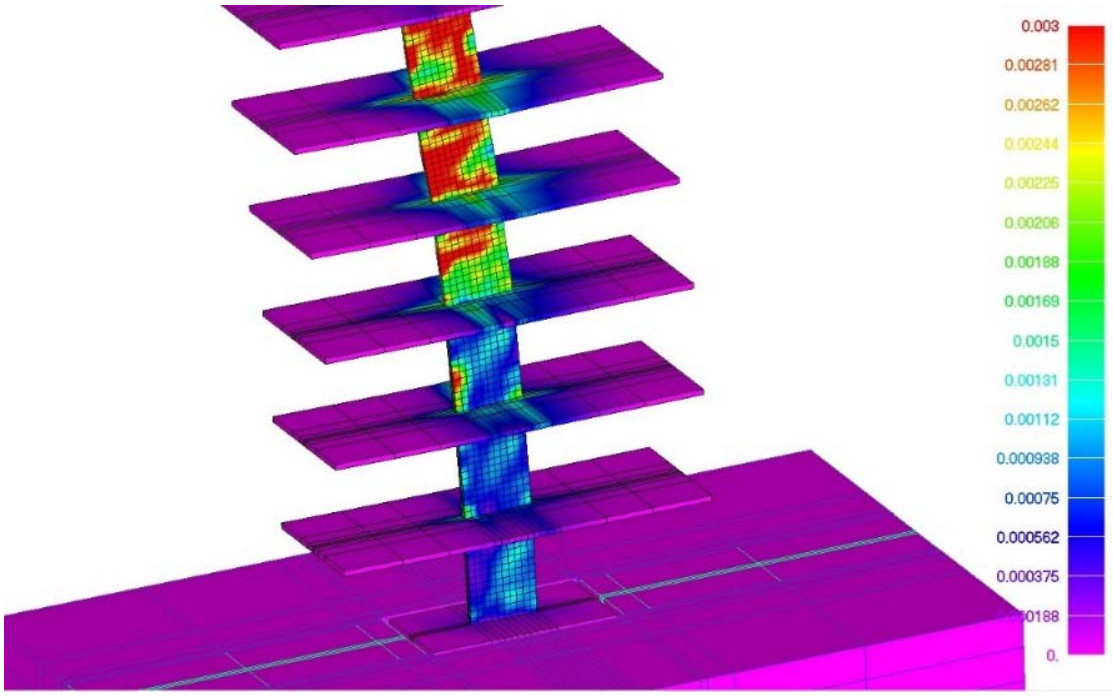

Figure 10- Von Mises strain contours for the SSI model at the 0.2m roof displacement step.

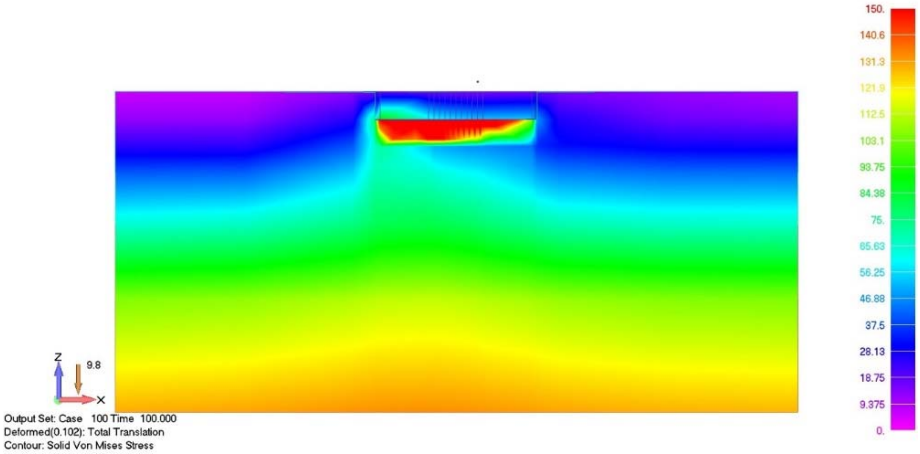

Figure 11- Von Mises stress contours for the soil domain at increment 100 (δ = 100 mm)

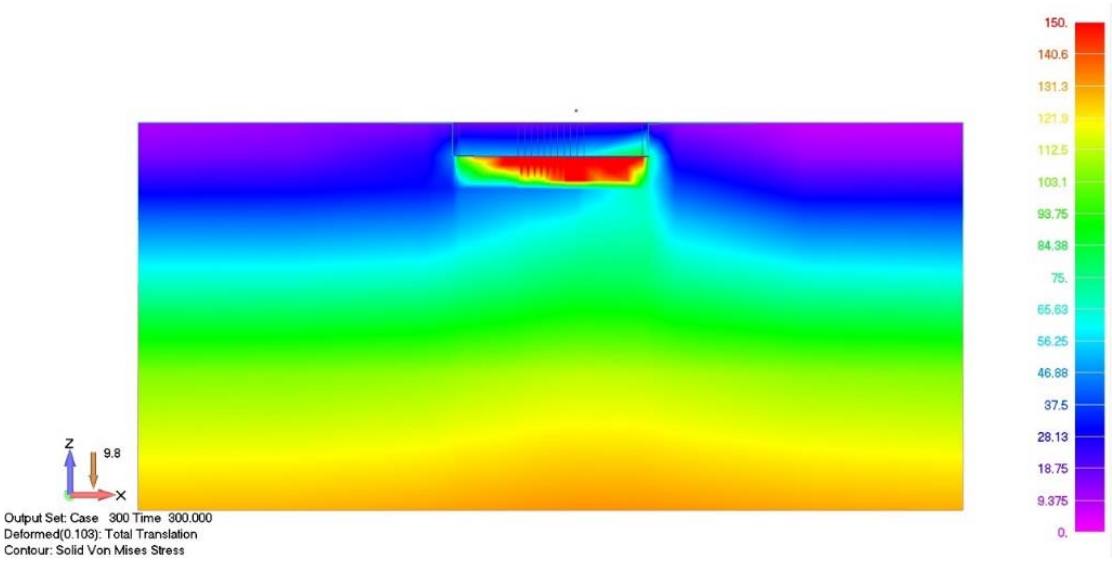

Figure 12- Von Mises stress contours for the soil domain at increment 300 (δ = -100 mm)

Based on the numerical findings, it was found that the isolated foundation did not develop any uplift thus the structure was compressing the soil medium-foundation interface throughout the cyclic analysis.

6 CONCLUSIONS

Based on the performed nonlinear FEA, the following may be concluded:

- The SSI affects the lateral response of structures by increasing lateral displacement. The weaker the soil, the higher the rotational release which the system will experience is. Thus, the difference in displacement between fixed and flexible base systems (for the same base shear) might not be felt if the soil is very stiff. i.e. when the soil is very stiff, the footing will not encounter relative displacement that will allow it to rotate.
- Regions of high strain concentrations shift when considering SSI effects. In fixed base systems, strains are higher at the bottom of the walls due to rotational fixity. Whereas in SSI system, walls behave in a more flexible manner deriving lower strain concentrations. However, the slabs will experience higher bending demands as the wall exhibits higher lateral displacements. Higher strain concentrations within the RC structural elements results in yielding of steel reinforcement, which is a limit state that requires further investigation.
- The shear wall of the SSI model develops lower strain concentrations in comparison to the fixed base model for the same horizontal deformation levels. This numerical finding could be attributed to the excess flexibility of the SSI model. This additional flexibility stems from the compressibility of the soil beneath the footing in response to the overturning effects of the imposed lateral displacements.
- The soil domain did not develop any nonlinearities throughout the cyclic analysis, and the footing did not develop any uplifts. The stress concentrations within the soil medium was found to be relatively low, highlighting the efficient footing design that did not allow for any high stress concentrations during the cyclic analysis.

7 REFERENCES

[1] H. Torabi and M. T. Rayhani, "Three dimensional Finite Element modeling of seismic soil–structure interaction in soft soil," *Computers and Geotechnics*, vol. 60, pp. 9–19, 2014.

[2] F. Behnamfar and M. Banizadeh, "Effects of soil-structure interaction on distribution of seismic vulnerability in RC structures," *Soil Dynamics and Earthquake Engineering*, vol. 80, pp. 73–86, 2016.

[3] G. Markou and M. AlHamaydeh, "3D Finite Element Modeling of GFRP-Reinforced Concrete Deep Beams without Shear Reinforcement," *International Journal of Computational Methods*, no. 1850001, DOI: 10.1142/S0219876218500019, 2017.

[4] G. Markou, R. Sabouni, F. Suleiman, and R. El-Chouli, "Full-Scale Modeling of the Soil-Structure Interaction Problem Through the use of Hybrid Models (HYMOD)," *International Journal of Current Engineering and Technology*, vol. 55, no. 22, pp. 2277–4106, 2015.

[5] M. AlHamaydeh, S. Yehia, N. Aly, A. Douba, and L. Hamzeh, "Design Alternatives for Lateral Force-Resisting Systems of Tall Buildings in Dubai, UAE," *International Journal of Civil and Environmental Engineering*, vol. 6, pp. 185–188, 2012.

[6] M. AlHamaydeh and G. Al-Shamsi, "Development of Analytical Fragility Curves for Representative Buildings in Dubai, United Arab Emirates," in *The International Conference on Earthquake Engineering; Skopje Earthquake - 50 Years of European Earthquake Engineering (SE-50EEE), May 29-31*, 2013.

[7] M. AlHamaydeh, N. Aly, and K. Galal, "Effect of Diverse Seismic Hazard Estimates on Design and Performance of RC Shear Wall Buildings in Dubai, UAE," in *The 2015 World Congress on Advances in Structural Engineering and Mechanics (ASEM15), August 25-29*, 2015.

[8] M. Al Satari and J. Anderson, "Estimating Inelastic Seismic Demands by Elastic Analysis for Reinforced Concrete (RC) Framed Structures," in *The 75th SEAOC Annual Convention, September 13-16*, 2006, pp. 153–167.

[9] M. Al Satari, *Estimation of Seismic Response Demands for R/C Framed Structures: An Insight Into The Nonlinear Seismic Behavior*. VDM Verlag, Saarbrücken, Germany, 2008.

[10] M. H. Al Satari, "Estimation of Seismic Response Demands for RC Framed Structures," University of Southern California, 2005.

[11] M. AlHamaydeh, K. Galal, and S. Yehia, "Impact of Lateral Force-Resisting System and Design/Construction Practices on Seismic Performance and Cost of Tall Buildings in Dubai, UAE," *Earthquake Engineering and Engineering Vibration*, vol. 12, no. 3, pp. 385–397, 2013.

[12] M. AlHamaydeh, N. Aly, and K. Galal, "Impact of Seismicity on Performance and Cost of RC Shear Wall Buildings in Dubai, UAE," *ASCE, Journal of Performance of Constructed Facilities*, no. DOI: 10.1061/(ASCE)CF.1943-5509.0001079, 2017.

[13] M. AlHamaydeh, J. Abdalla, S. Abdalla, A. Al-Rahmani, and A. Mostafa, "Inelastic Seismic Demands For Reinforced Concrete Frames In Dubai," in *The 14th European Earthquake Engineering Conference (14EEEC), Aug. 30-Sept. 3*, 2010.

[14] J. Anderson, V. Bertero, and M. Al Satari, "Inelastic Seismic Response of a Tilt-up Wall Building and Design Implications," in *The 74th SEAOC Annual Convention, Sept. 28-Oct. 1*, 2005.

[15] M. Al Satari and J. Anderson, "Nonlinearity Effects on the Seismic Behavior of RC Framed Structures," in *The 76th SEAOC Annual Convention, September 26-29*, 2007.

[16] M. AlHamaydeh, S. Abdullah, A. Hamid, and A. Mustapha, “Seismic design factors for RC special moment resisting frames in Dubai, UAE,” *Earthquake Engineering and Engineering Vibration*, vol. 10, no. 4, pp. 495–506, 2011.
[17] J. C. Anderson, V. V. Bertero, M. Kargahi, and M. Al Satari, “Seismic Performance of an Instrumented Tilt-up Wall Building,” Pacific Earthquake Engineering Research Center, Berkeley, California, USA, 2004.
[18] M. AlHamaydeh, N. Ibrahim, D. Kaloti, O. Alhasan, and A. Aisha, “Structural Design of Steel Plate Shear Wall Systems in Dubai, UAE,” in *CYRUS Institute of Knowledge (CIK) conference, "West-Meets-East: Exploring Sustainable Development, Innovation, and Entrepreneurship Opportunities, January 9-11*, 2014.
[19] M. AlHamaydeh, F. Abed, and A. Mostafa, “Finite Element Simulation of Different Failure Modes for Buckling-Restrained Braces under Cyclic Loading,” in *The 9th International Conference on Composite Science and Technology (ICCST-9), April 24-26*, 2013.
[20] M. AlHamaydeh, F. Abed, and A. Mustapha, “Key parameters influencing performance and failure modes for BRBs using nonlinear FEA,” *Journal of Constructional Steel Research*, vol. 116, pp. 1–18, Jan. 2016.
[21] A. M. Reinhorn, H. Roh, M. Sivaselvan, S. K. Kunnath, R. E. Valles, A. Madan, C. Li, R. Lobo, and Y. J. Park, “IDARC2D Version 7.0: A Program for the Inelastic Damage Analysis of Structures,” 2009.
[22] M. AlHamaydeh, M. Najib, and S. Alawnah, “INSPECT: A Graphical User Interface Software Package for IDARC-2D,” *SoftwareX*, vol. 5, pp. 243–251, 2016.
[23] F. McKenna, G. Fenves, and M. Scott, “OpenSees – Open System for Earthquake Engineering Simulation, ver. 2.5.0.” Pacific Earthquake Engineering Research Center (PEER), http://opensees.berkeley.edu/, Berkeley, California, USA, 2016.
[24] A. Schellenberg, T. Yang, and E. Kohama, “OpenSees Navigator ver. 2.5.5.” Pacific Earthquake Engineering Research Center (PEER), http://openseesnavigator.berkeley.edu/, Berkeley, California, USA, 2015.
[25] S. Mazzoni, “BuildingTcl/BuildingTclViewer.” Pacific Earthquake Engineering Research Center (PEER), http://opensees.berkeley.edu/wiki/index.php/BuildingTcl, Berkeley, California, USA, 2010.
[26] A. S. Elnashai, V. Papanikolaou, and D. Lee, “ZEUS NL – A system for Inelastic Analysis of Structures, User’s Manual, ver. 1.9.0.” Mid-America Earthquake (MAE) Center, Department of Civil and Environmental Engineering, University of Illinois at Urbana-Champaign, http://mae.cee.illinois.edu/software/software_zeusnl.html, Urbana-Champaign, Illinois, USA, 2011.
[27] SeismoSoft Inc., “SeismoStruct 2016 – A Computer Software for Static and Dynamic Nonlinear Analysis of Framed Structures, ver. 7.” SeismoSoft, Inc., http://www.seismosoft.com/SeismoStruct_2016_Release-4_ENG, 2016.
[28] ASCE/SEI, “Minimum Design Loads for Buildings and Other Structures (ASCE/SEI 7-10),” American Society of Civil Engineers/Structural Enginnering Institute, 2010.
[29] G. Markou, “ReConAn - Finite Element Analysis Software, v1.00.” Institute of Structural Analysis and Seismic Research, National Technical University of Athens, 2010.
[30] M. Ghandil and F. Behnamfar, “The near-field method for dynamic analysis of structures on soft soils including inelastic soil-structure interaction,” *Soil Dynamics and Earthquake Engineering*, vol. 75, pp. 1–17, 2015.
[31] B. M. Das, *Principles of geotechnical engineering*. Cengage Learning, 2010.
[32] H. Lin, M. T. Suleiman, H. M. Jabbour, D. G. Brown, and E. Kavazanjian, “Enhancing

the Axial Compression Response of Pervious Concrete Ground Improvement Piles Using Biogrouting," *Journal of Geotechnical and Geoenvironmental Engineering*, vol. 142, no. 10, p. 4016045, Oct. 2016.

[33] A. S. Elnashai and L. Di Sarno, *Fundamentals of Earthquake Engineering*, First Edit. John Wiley & Sons Ltd, 2008.

[34] ACI Committee 318, *Building Code Requirements for Structural Concrete (ACI 318M-11)*. 2011.

[35] C. Mourlas, M. Papadrakakis, and G. Markou, "A Computationally Efficient Model For The Cyclic Behavior Of Reinforced Concrete Structural Members," pp. 1–40, 2017.